Optimum design of skeletal structures using PSO-Based algorithms

A. Kaveh*. M. Ilchi Ghazaan

Centre of Excellence for Fundamental Studies in Structural Engineering, Iran University of Science and Technology, Narmak, Tehran, P.O. Box 16846-13114, Iran

Abstract: The particle swarm optimization with an aging leader and challengers (ALC-PSO) algorithm is a recently developed optimization method which transplants the aging mechanism to PSO. The ALC-PSO prevents premature convergence and maintains the fast-converging feature of PSO. In this paper, a harmony search-based mechanism is used to handle the side constraints and it is combined with ALC-PSO, resulting in a new algorithm called HALC-PSO. These two algorithms are employed to optimize different types of skeletal structures with continuous and discrete variables. The results are compared to those of some other meta-heuristic algorithms.

Keywords: Particle swarm optimization; aging mechanism; challengers; harmony search; algorithm; trusses; frames.

1. Introduction

Optimal design of engineering problems has received a great deal of attention in the recent decades. The aim of these problems is to minimize an objective function that is often the cost of the structure or a quantity directly proportional to the cost under certain constraints that may correspond to different engineering demands like stresses, displacements, maximum inter-story drift and other requirements.

The recent generation of the optimization methods comprises of meta-heuristic algorithms that are proposed to solve complex problems. A meta-heuristic method often consists of a group of search agents that explore the feasible region based on both randomization and some specified

*Corresponding author at: Centre of Excellence for Fundamental Studies in Structural Engineering, Iran University of Science and Technology, Narmak, Tehran, P.O. Box 16846-13114, Iran. Tel.: +98 21 77240104; fax: +98 21 77240398.
E-mail address: alikaveh@iust.ac.ir (A. Kaveh).

rules (Kaveh [1]). The basic idea behind these stochastic search techniques is to simulate natural phenomena such as survival of the fittest, swarm intelligence and the cooling process of molten metals into a numerical algorithm. These algorithms are named according to the natural phenomenon used in the construction of the method (Dogˇan and Saka [2]). Genetic algorithm (GA) is inspired by Darwin's theory about biological evolutions (Holland [3]; Goldberg [4]). Particle swarm optimization (PSO) simulates the social interaction behavior of the birds flocking and fish schooling (Eberhart and Kennedy [5]; Kennedy and Eberhart [6]). Ant colony optimization (ACO) imitates the manner that ant colonies find the shortest route between the food and their nest (Dorigo et al. [7]). Simulated annealing (SA) utilizes energy minimization that happens in the cooling process of molten metals (Kirkpatrick et al. [8]). Harmony search (HS) algorithm was conceptualized using the musical process of searching for a perfect state of harmony (Geem [9]). Charged system search (CSS) uses the electric laws of physics and the Newtonian laws of mechanics to guide the charged particles (Kaveh and Talatahari [10]). Firefly algorithm (FA) is based on the flashing patterns and behaviors of fireflies (Yang [11]). Ray Optimization (RO) is based on the Snell's light refraction law when light travels from a lighter medium to a darker medium (Kaveh and Khayatazad [12]). Ant lion optimizer (ALO) mimics the hunting mechanism of ant lions in nature (Mirjalili [13]).

In this article, two PSO-based algorithms are utilized for optimal design of skeletal structures. PSO is a population-based algorithm that has some advantages such as few parameters implementation, easy programming for computer, effective exploration of global solutions for some hard problems, and fast-converging behavior. However ***gBest***, the historically best position of the entire swarm, leads all particles and when trapped at a local optimum may lead the entire swarm to that point resulting in a premature convergence. The PSO with an aging leader and challengers (ALC-PSO) algorithm, developed by Chen et al. [14], utilizes the aging theory in the particle swarm optimization to overcome this problem. ALC-PSO is characterized by assigning the leader of the swarm with a growing age and a lifespan. The lifespan is adaptively adjusted according to the leader's leading power. If a leader shows strong leading power, it lives longer to attract the swarm toward better positions and once the leader reaches a local optimum, it fails to improve the quality of the swarm and gets aged quickly. In this case, new challengers emerge to replace the old leader resulting in diversity. By adding these mechanisms to PSO, the fast-converging feature can be preserved. On the other hand, ALC-PSO has the ability to escape from local optima preventing premature convergence (Chen et al. [14]). The other method is harmony aging leader challenger particle swarm optimization (HALC-PSO) which utilizes HS algorithm in ALC-PSO for handling side constraints (Kaveh and Ilchi Ghazaan [15]).

These two algorithms are employed to optimize different types of skeletal structures consisting of trusses and frames, with continuous and discrete variables. The design constraints are imposed according to the provisions of ASD-AISC (Allowable Stress Design, American Institute of Steel Construction) for truss structures (AISC [16]) and LRFD-AISC (Load and Resistance Factor Design) for frame structures (AISC [17]). Optimization results are compared to those of some other meta-heuristic algorithms. It appears that the proposed PSO variants are quite suitable for structural engineering problems.

2. Optimum design of skeletal structures

Size optimization of skeletal structures is known as benchmark in the field of optimization problems. The mathematical formulation of these problems can be expressed as:

$$\begin{aligned}
&\text{Find} && \{X\}=[x_1,x_2,..,x_{ng}] \\
&\text{to minimize} && W(\{X\})=\sum_{i=1}^{nm}\rho_i A_i L_i \\
&\text{subjected to:} && \begin{cases} g_j(\{X\})\le 0, \quad j=1,2,...,nc \\ \mathrm{x}_{\mathrm{i\,min}} \le x_{\mathrm{i}} \le x_{i\max} \end{cases}
\end{aligned} \tag{1}$$

where $\{X\}$ is the vector containing the design variables; ng is the number of design variables; $W(\{X\})$ presents weight of the structure; nm is the number of elements of the structure; ρ_i, A_i and L_i denote the material density, cross-sectional area, and the length of the ith member, respectively. x_{imin} and x_{imax} are the lower and upper bounds of the design variable x_i, respectively. $g_j(\{X\})$ denotes design constraints; and nc is the number of the constraints.

In order to handle the constraints, the penalty approach is employed (Kaveh and Talatahari [18]). Thus, the objective function is redefined as follows:

$$f(\{X\}) = (1+\varepsilon_1.\upsilon)^{\varepsilon_2} \times W(\{X\}) \tag{2}$$

where υ denotes the sum of the violations of the design constraints. The constant ε_1 is set to unity and ε_2 is set to 1.5 and ultimately increased to 3. Such a scheme penalizes the unfeasible solutions more severely as the optimization process proceeds.

Design constraints for truss and frame structures, studied in this paper, are briefly explained in the following sections.

2.1.Constraint conditions for truss structures

The stress and stability limitations of the members are imposed according to the provisions of ASD-AISC [16] as follows:

The allowable tensile stresses for tension members are calculated as:

$$\sigma_i^+ = 0.6\mathrm{F_y} \tag{3}$$

where F_y stands for the yield strength.

The allowable stress limits for compression members are calculated depending on two possible failure modes of the members known as elastic and inelastic buckling:

$$\sigma_i^- = \begin{cases} \left[\left(1-\dfrac{\lambda_i^2}{2C_c^2}\right)F_y\right] \Big/ \left[\dfrac{5}{3}+\dfrac{3\lambda_i}{8C_c}-\dfrac{\lambda_i^3}{8C_c^3}\right] & \text{for } \lambda_i < C \\ \dfrac{12\pi^2 E}{23\lambda_i^2} & \text{for } \lambda_i \geq C_c \end{cases} \tag{4}$$

where E is the modulus of elasticity; λ_i is the slenderness ratio $\left(\lambda_i = kl_i/r_i\right)$; C_c denotes the slenderness ratio dividing the elastic and inelastic buckling regions ($c_c = \sqrt{2\pi^2 E/F_y}$); k is the effective length factor (k is set 1 for all truss members); L_i is the member length; and r_i is the minimum radius of gyration.

In this design code provisions, the maximum slenderness ratio is limited to 300 for tension members, and it is recommended to be 200 for compression members. The other constraint corresponds to the limitation of the nodal displacements:

$$\delta_i - \delta_i^u \le 0 \qquad i = 1,\ 2,\ \dots,\ nn \tag{5}$$

where δ_i is the nodal deflection; δ_i^u is the allowable deflection of node i; nn is the number of nodes.

2.2. Constraint conditions for frame structures

Design constraints according to LRFD-AISC [17] requirements can be summarized as follows:

(a) Maximum lateral displacement:

$$\frac{\Delta_T}{H} - R \le 0 \tag{6}$$

where Δ_T is the maximum lateral displacement; H is the height of the frame structure; R is the maximum drift index (1/300).

(b) The inter-story displacements:

$$\frac{d_i}{h_i} - R_I \le 0, \quad i = 1, 2, \dots, ns \tag{7}$$

where d_i is the inter-story drift; h_i is the story height of the ith floor; ns is the total number of stories; R_I is the inter-story drift index which is equal to 1/300.

(c) Strength constraints:

$$\begin{cases} \dfrac{P_u}{2\phi_c P_n} + \dfrac{M_u}{\phi_b M_n} - 1 \le 0, & for\ \dfrac{P_u}{\phi_c P_n} < 0.2 \\ \dfrac{P_u}{\phi_c P_n} + \dfrac{8M_u}{9\phi_b M_n} - 1 \le 0, & for\ \dfrac{P_u}{\phi_c P_n} \ge 0.2 \end{cases} \tag{8}$$

where P_u is the required strength (tension or compression); P_n is the nominal axial strength (tension or compression); φ_c is the resistance factor (φ_c = 0.9 for tension, φ_c = 0.85 for compression); M_u is the required flexural strength; M_n is the nominal flexural strengths; and φ_b denotes the flexural resistance reduction factor (φ_b = 0.90). The nominal tensile strength for yielding in the gross section is computed as:

$$P_n = A_g . F_y \tag{9}$$

The nominal compressive strength of a member is computed as:

$$P_n = A_g . F_{cr} \tag{10}$$

$$\begin{cases} F_{cr} = (0.658^{\lambda_c^2}) F_y, & for \lambda_c \le 1.5 \\ F_{cr} = (\dfrac{0.877}{\lambda_c^2}) F_y, & for \lambda_c > 1.5 \end{cases} \tag{11}$$

$$\lambda_c = \frac{kl}{r\pi}\sqrt{\frac{F_y}{E}} \tag{12}$$

where A_g is the cross-sectional area of a member, and k is the effective length factor determined by the approximated formula (Dumonteil [19]):

$$k = \sqrt{\frac{1.6G_A G_B + 4.0(G_A + G_B) + 7.5}{G_A + G_B + 7.5}} \tag{13}$$

where G_A and G_B are stiffness ratios of columns and girders at two end joints, A and B, of the column section being considered, respectively.

3. **Optimization algorithms**

Particle swarm optimization (PSO), introduced by Eberhart and Kennedy [5], is a population-based method inspired by the social behavior of animals such as fish schooling and bird flocking. The PSO algorithm is initialized with a population of random candidate solutions in an *n*-dimensional search space, conceptualized as particles. Each particle in the swarm maintains a velocity vector and a position vector. During each generation, each particle updates its velocity and position by learning from the best position achieved so far by the particle itself and the best position achieved so far across the whole population. Let $V_i(v_i^1, v_i^2, \ldots, v_i^n)$ and $X_i(x_i^1, x_i^2, \ldots, x_i^n)$ be the ith particle's velocity vector and position vector, respectively, and M be the number of particles in a population. The update rules in the PSO algorithm are based on the following two simple equations (Shi and Eberhart [20]):

$$v_i^j \leftarrow \omega . v_i^j + \mathrm{c}_1 . \mathrm{r}_1^j . (\mathrm{pBest}_i^j - \mathrm{x}_i^j) + \mathrm{c}_2 . \mathrm{r}_2^j . (\mathrm{gBest}^j - \mathrm{x}_i^j) \tag{14}$$

$$x_i^j \leftarrow x_i^j + v_i^j \tag{15}$$

where ω is an inertia weight, $\boldsymbol{pBest_i}(pBest_i^1, pBest_i^2, \ldots, pBest_i^n)$ is the historically best position of particle i ($i = 1, 2, \ldots, M$), $\boldsymbol{gBest}(gBest^1, gBest^2, \ldots, gBest^n)$ is the historically best position of the entire swarm, r_1^j and r_2^j are two random numbers uniformly distributed in the range of [0,1], c_1 and c_2 are two parameters to weigh the relative importance of $\boldsymbol{pBest_i}$ and ***gBest***, respectively and $j (j=1, 2, \ldots, n)$ represents the jth dimension of the search space.

The PSO algorithm has very few parameters to adjust, which makes it particularly easy to implement and it is effective to explore global solutions for a variety of difficult optimization problems. Another advantage of PSO is that all particles learn from ***gBest*** in updating velocities and positions so the algorithm exhibits a fast-converging behavior. However, on multimodal problems, a ***gBest*** located at a local optimum may trap the whole swarm leading to premature convergence (Chen et al. [14]). Different variants of PSO have been developed to improve its performance and two of them are described in the following sections.

3.1. Particle swarm optimization with an aging leader and challengers

In nature, when the leader of a colony gets too old to lead, new individuals emerge to challenge and claim the leadership. In this way, the community is always led by a leader with adequate leading power. Inspired by this natural phenomenon, Aging mechanism has been transplanted into PSO leading to ALC-PSO (Chen et al. [14]). In this method, the leader of the swarm ages and has a limited lifespan that is adaptively tuned according its leading power. When the lifespan is exhausted, the leader is challenged and replaced by newly generated particles. Therefore, the leader in ALC-PSO is not necessarily the ***gBest***, but a particle with adequate leading power guaranteed by the aging mechanism. In this way, ALC-PSO prevents the premature convergence and maintaining the fast-converging feature of the PSO. Let us change ***gBest*** into ***Leader*** in the velocity update rule of the PSO as:

$$v_i^j \leftarrow \omega . v_i^j + \mathrm{c}_1.\mathrm{r}_1^{\mathrm{j}}.(\mathrm{pBest}_{\mathrm{i}}^{\mathrm{j}} - \mathrm{x}_{\mathrm{i}}^{\mathrm{j}}) + \mathrm{c}_2.\mathrm{r}_2^{\mathrm{j}}.(\mathrm{Leader}^{\mathrm{j}} - \mathrm{x}_{\mathrm{i}}^{\mathrm{j}}) \tag{16}$$

This technique consists of the following steps:

Level 1: Initialization

Step 1: ALC-PSO parameters are set. The initial locations of particles are created randomly in an *n*-dimensional search space and their associated velocities are set to 0. The best particle is selected as the ***Leader***. Its age θ and lifespan Θ are initialized to 0 and Θ_0 , respectively.

Level 2: Search

Step 1: Velocities are updated according to Eq. (16) and each particle moves to the new position based on its previous position and updated velocity as specified in Eq. (15).

Step 2: The historically best position X_i (i = 1, 2, …, M) of each particle is saved as its ***Pbest$_i$***. Moreover, if the best location found in this iteration is better than the ***Leader***, then the ***Leader*** is updated.

Step 3: The ***Leader*** lifespan is updated by the following formulas during a Leader's lifetime (i.e., θ =0, 1, …, Θ):

$$\delta_{gBest}(\theta) = f(gBest(\theta)) - f(gBest(\theta - 1)) < 0, \qquad \theta = 1,2,...,\Theta \tag{17}$$

$$\sum_{i=1}^{M} \delta_{pBest_i}(\theta) = \sum_{i=1}^{M} f\,(pBest_i(\theta)) - \sum_{i=1}^{M} f\,(pBest_i(\theta-1)) < 0, \qquad \theta = 1,2,...,\Theta \tag{18}$$

$$\delta_{Leader}(\theta) = f\,(Leader(\theta)) - f\,(Leader(\theta-1)) < 0, \qquad \theta = 1,2,...,\Theta \tag{19}$$

where ***gBest*** and *f* (***gBest***(θ)) are the historically best solution and its objective function value when the age of the Leader is θ, respectively. These formulas create four cases:

I. Good Leading Power: If Eq. (17) is satisfied, it can be deduced that Eq. (18) and Eq. (19) also hold. Hence, the current ***Leader*** has a strong leading power to improve the swarm. Therefore, the lifespan Θ is increased by 2.

II. Fair Leading Power: If only Eqs. (18) and (19) are satisfied, the lifespan Θ is increased by 1 because it can be deduced that the current ***Leader*** still has potential to improve the swarm in the following iterations.

III. Poor Leading Power: If only Eq. (19) is satisfied, the lifespan Θ remains unchanged since the current ***Leader*** only has the ability to improve itself.

IV. No Leading Power: If none of the above formulas is satisfied, it demonstrates that the current ***Leader*** is not able to improve the swarm in the subsequent iterations. Therefore, the lifespan Θ decreased by 1.

After the lifespan Θ is adjusted, the age θ of the ***Leader*** is increased by 1. If the lifespan is exhausted, i.e., $\theta \geq \Theta$, go to Step 4. Otherwise, go to Level 3.

Step 4: A new particle that is called ***Challenger*** has to be created to challenge and try to replace the old ***Leader***. With probability like *pro*, $Challenger^j$ is determined randomly in the jth dimension. Otherwise, $Challenger^j$ is inherited from the Leader:

$$Challenger^{\,j} = \begin{cases} random(L^j, U^j), & rnd_j < pro \\ Leader^{\,j}, & otherwise, \end{cases} \qquad j = 1,2,...,n \tag{20}$$

where L^j and U^j are the lower and upper bounds of the j-th design variable, respectively. *rnd* is a random number in the interval [0,1]. In this paper, *pro* is set to $1/n$. If the

Challenger is exactly the same as the previous ***Leader***, one dimension of ***Challenger*** is randomly selected and its value is set at random with in its domain.

Step 5: The ***Challenger*** is utilized as a temporary ***Leader*** for *T* iterations to evaluate its leading power. In these *T* iterations, the velocity is updated by:

$$v_i^j \leftarrow \omega . v_i^j + \mathrm{c}_1 . \mathrm{r}_1^{\mathrm{j}} . (\mathrm{pBest}_{\mathrm{i}}^{\mathrm{j}} - \mathrm{x}_{\mathrm{i}}^{\mathrm{j}}) + \mathrm{c}_2 . \mathrm{r}_2^{\mathrm{j}} . (\mathrm{Challenger}^{\mathrm{j}} - \mathrm{x}_{\mathrm{i}}^{\mathrm{j}}) \quad (21)$$

The ***Challenger*** is accepted as ***Leader*** if any ***pBest*** is improved during these *T* iterations and its age θ and lifespan Θ are respectively set to 0 and Θ_0. Otherwise, the previous ***Leader*** is used and its lifespan Θ remains unchanged and its age θ is reset to $\theta = \Theta$-1.

Level 3: Terminal condition check

Step 1: After the predefined maximum evaluation number, the optimization process is terminated.

3.2. Harmony search added to ALC-PSO

In order to deal with the case of an agent violating side constraints is an important issue in most of the meta-heuristic algorithms. One of the simplest approaches is utilizing the nearest limit values for the violated variable. Alternatively, one can force the violating particle to return to its previous position, or one can reduce the maximum value of the velocity to allow fewer particles to violate the variable boundaries. Although these approaches are simple, they are not sufficiently efficient and may lead to reduce the exploration of the search space (Kaveh and Talatahari [10]).

This problem has previously been addressed and solved using the harmony search-based handling approach (Kaveh and Talatahari [21]; [22]; [10]). In this technique, there is a possibility like *HMCR* (harmony memory considering rate) that specifies whether the violating component must be selected randomly from ***pBest*** or it should be determined randomly in the search space. So if x_i^j is the *j*th component of the *i*th particle which violates the boundary limitation, it must be regenerated by the following formula:

$$x_i^j = \begin{cases} w.p.\, HMCR; & \rightarrow \quad Select\ a\ new\ value\ for\ a\ variable\ from\ pBest_k^j \\ & \qquad \rightarrow w.p.\,(1-PAR)\ do\ nothing, \\ & \qquad \rightarrow w.p.\,PAR\ choose\ a\ neighboring\ value, \\ w.p.\,(1-HMCR) & \rightarrow \quad Select\ a\ new\ value\ randomly \end{cases} \tag{22}$$

where "*w.p.*" is the abbreviation for "with the probability" and *PAR* is the pitch adjusting rate which varies between 0 and 1. k is identified randomly from [1, *M*] (*M* be the number of particles). By adding this variable constraint handling approach to ALC-PSO, the HALC-PSO algorithm is developed.

4. Test problems and discussion of optimization results

Four skeletal structures are optimized for minimum weight with the cross-sectional areas of the members being the design variables to verify the efficiency of the present methods. The parameters of ALC-PSO and HALC-PSO are set as follows: c_1 and c_2 are both set to 2; ω is set to 0.4; the legal velocity range V_{max} is considered 50% of the search range; Θ_0 and T are respectively set to 60 and 2. In HALC-PSO, *HMCR* is taken as 0.95 and *PAR* is set to 0.10. The population of 30 particles are utilized in test examples 1,2 and 4, while there are only 15 particles in test problem 3. To reduce statistical errors, each test is repeated 30 times independently. For each independent run, 20,000 evaluations are considered as maximum function evaluations in test examples 1, 3 and 4 while in the case of test problem 2 it is set equal to 30,000.

In the discrete problems, particles are allowed to select discrete values from the commercially available cross sections (real numbers are rounded to the nearest integer in each iteration). This method is chosen due to its easy computer implementation. The algorithms are coded in MATLAB and the structures are analyzed using the direct stiffness method.

4.1. Spatial 120-bar dome shaped truss

The schematic and element grouping of the spatial 120-bar dome truss are shown in Fig. 1. For clarity, not all the element groups are numbered in this figure. The 120 members are categorized into seven groups because of symmetry. The modulus of elasticity is 30,450 ksi (210 GPa) and the material density is 0.288 lb/in^3 (7971.810 kg/m^3). The yield stress of steel is taken as 58.0 ksi

(400 MPa). The dome is considered to be subjected to vertical loading at all the unsupported joints. These loads are taken as −13.49 kips (−60 kN) at node 1, −6.744 kips (−30 kN) at nodes 2 through 14, and −2.248 kips (−10 kN) at the all other nodes. Element cross-sectional areas can vary between 0.775 in^2 (5 cm^2) and 20.0 in^2 (129.032 cm^2). Constraints on member stresses are imposed according to the provisions of ASD-AISC [16], as defined by Eqs. (3,4). Displacement limitations of ±0.1969 in (±5 mm) are imposed on all nodes in x, y and z coordinate directions.

Table 1 shows the best solution vectors, the corresponding weights, the average weights and the Standard deviation for present algorithms and some other meta-heuristic algorithms. It can be seen from Table 1 that the best design is obtained by HALC-PSO which is 33250.01 lb. ICA (Kaveh and Talatahari [18]), CSS (Kaveh and Talatahari [23]) and IRO (Kaveh et al. [24]) algorithms found the best solution after 6,000, 7,000 and 18,300 structural analyses, respectively. ALC-PSO and HALC-PSO achieved the optimum design after 10,000 and 13,000 structural analyses, respectively. However, they can obtain the ICA and IRO optimized designs after about 5,500 structural analyses and CSS optimized designs after about 7,000 structural analyses. Fig. 2 compares the best and average convergence history for the present algorithms.

4.2. Spatial 582-bar tower

The second test problem regards the spatial 582-bar tower truss with the height of 3149.6 in (80 m), shown in Fig. 3. The tower is optimized for minimum volume with the cross-sectional areas of the members being the design variables. The symmetry of the tower about x-axis and y-axis is considered to group the 582 members into 32 independent sizing variables. A single load case is considered consisting of the lateral loads of 1.12 kips (5.0 kN) applied in both x- and y-directions and a vertical load of -6.74 kips (-30 kN) applied in the z-direction at all nodes of the tower. A discrete set of standard steel sections selected from W-shape profile list based on area and radii of gyration properties is used to size the variables. The lower and upper bounds of sizing variables are taken as 6.16 in^2 (39.74 cm^2) and 215.0 in^2 (1387.09 cm^2), respectively (Hasancebi et al. [25]). The stress and stability limitations of the members are imposed according to the provisions of ASD-AISC [16]. Furthermore, nodal displacements in all coordinate directions must be smaller than ±3.15 in (±8.0 cm).

Optimization results are presented in Table 2. ALC-PSO obtained the lightest design overall. HALC-PSO obtained the second best design, which is only 0.5% larger than its counterpart found by ALC-PSO. The optimized volumes of DHPSACO (Kaveh and Talatahari [26]) and BB-BC (Kaveh and Talatahari [27]), respectively, are 4% and 5.4% larger than that of ALC-PSO. DHPSACO, BB-BC, ALC-PSO and HALC-PSO required 8,500, 12,500, 15,000 and 16,000 structural analyses to converge to the optimum, respectively. However, the proposed method can obtain the DHPSACO and BB-BC optimized designs after about 5,500 and 5,000 structural analyses, respectively. Fig. 4 shows that the maximum element stress ratio evaluated at the optimum design for ALC-PSO and HALC-PSO is 99.87% and 99.34%, respectively. Nodal displacements evaluated at the optimized designs are shown in Figs. 5 through 7. Some stress and displacement constraint margins evaluated for ALC-PSO and HALC-PSO are critical.

4.3. Three-bay fifteen-story frame

The schematic, applied loads and the numbering of member groups for this test problem are shown in Fig. 8. This frame consists of 64 joints and 105 members. The displacement and AISC-LRFD combined strength constraints are the performance constraint of this example (AISC [17]). An additional constraint of displacement control is the sway of the top story that is limited to 9.25 in (23.5 cm). The material has a modulus of elasticity equal to E=29,000 ksi (200 GPa) and a yield stress of F_y=36 ksi (248.2 MPa). The effective length factors of the members are calculated as $k_x \geq 0$ for a sway-permitted frame and the out-of-plane effective length factor is specified as k_y=1.0. Each column is considered as non-braced along its length, and the non-braced length for each beam member is specified as one-fifth of the span length.

Table 3 compares the designs developed by HBB-BC (Kaveh and Talatahari [27]), ICA (Kaveh and Talatahari [18]) and the present algorithms. It can be seen that the HALC-PSO designs a structure that is 11%, 8% and 0.2% lighter than the HBB-BC, ICA and ALC-PSO, respectively. HBB-BC and ICA found the best solution after 9,500 and 6,000 structural analyses, respectively. ALC-PSO and HALC-PSO, respectively, require 13,395 and 9,390 analyses to converge to their best designs. However, they can obtain the ICA optimized design after about 2,000 analyses. The average optimal weights of ALC-PSO and HALC-PSO for the 30 independent runs are 88,330 lb and 88,114 lb, respectively. The convergence curves of the present algorithms for the best and average optimum designs are compared in Fig. 9.

4.4. Three-bay twenty four-story frame

Fig. 10 shows the structural scheme, service loading conditions and member group numbering of the three-bay twenty four-story frame as the last test problem in this study (Degertekin [28]). This frame consists of 100 joints and 168 members. The member grouping results in 16 column sections and 4 beam sections for a total of 20 design variables. In this example, each of the four beam element groups is chosen from all 267 W-shapes, while the 16 column member groups are selected from only W14 sections. The material has a modulus of elasticity equal to E=29,732 ksi (205 GPa) and a yield stress of F_y=33.4 ksi (230.3MPa). The frame is designed following the AISC-LRFD specifications (AISC [17]). The effective length factors of the members are calculated as $k_x \geq 0$ for a sway-permitted frame and the out-of-plane effective length factor is specified as k_y=1.0. All columns and beams are considered as non-braced along their lengths.

Results of the present study and some meta-heuristic techniques are provided in Table 4. It can be seen that best design is found by using HALC-PSO which is 201,906 lb. The optimized weights of ACO (Camp et al. [29]), HS (Degertekin [28]), ICA (Kaveh and Talatahari [18]) and ALC-PSO, respectively, are 8.4%, 6.0%, 5.3%, and 0.2% larger than that of HALC-PSO. The ICA required 7,500 structural analyses to converge to the optimal solution, which is less than number of analyses required by other methods. Here, 13,000 analyses were required by ALC-PSO and 18,000 analyses by HALC-PSO. However, they can obtain the ICA optimized design after about 5,500 analyses. Member stress ratio values computed at the optimized design are shown in Fig. 11. The maximum values of the stress ratio for ALC-PSO and HALC-PSO are 96.64% and 96.91%, respectively. Fig. 12 shows the inter-story drift constraint margins. It can be seen that the inter-story in many stories for ALC-PSO and HALC-PSO are close to the allowable values.

5. Concluding remarks

In this study, the particle swarm optimization with an aging leader and challengers is employed for size optimization of skeletal structures. Also, a new meta-heuristic algorithm so-called HALC-PSO is developed to improve the performance of the ALC-PSO method. This technique applies Harmony Search to handle the side constraints.

The merits of these two algorithms lie in three aspects. First, the whole swarm is attracted by a leader with adequate leading power just like what the ***gBest*** does in the PSO. Thus, the fast converging feature of the PSO is preserved. Second, when a leader has poor leading power, gets aged quickly and new challengers emerge to replace the old leader. Therefore, the algorithm can maintain diversity and prevent premature convergence. Finally, the proposed algorithms still have a simple structure because the mechanisms added to PSO are conceptually simple.

The efficiency of ALC-PSO and HALC-PSO is investigated to find optimum design of truss and frame structures with continuous and discrete variables. Optimization results are compared to those of some other well-known meta-heuristics. The optimum design obtained by HALC-PSO is lighter than other methods in three of four examples, and its reliability of search is shown through statistical information. The convergence rate of ALC-PSO and HALC-PSO are approximately identical, and better than other methods. To sum up, optimization results confirm the validity of the proposed approaches.

References

[1] Kaveh, A. Advances in Metaheuristic Algorithm for Optimal design of Structures, Springer, Awitzerland, (2014).

[2] Dogˇan, E., and Saka, M. P. Optimum design of unbraced steel frames to LRFD-AISC particle swarm optimization. *Advances in Engineering Software*, 46, pp. 27-34, (2012).

[3] Holland, J. H. Adaptation in natural and artificial systems. Ann Arbor: University of Michigan, (1975).

[4] Goldberg, D.E. Genetic algorithms in search optimization and machine learning. Boston: Addison-Wesley, (1989).

[5] Eberhart, R. C., and Kennedy, J. A new optimizer using particle swarm theory. *In Proceedings of the 6th International Symposum in Micromach. Hum. Science*, pp. 39– 43, (1995).

[6] Kennedy, J., and Eberhart, R.C. Particle swarm optimization. *In Proceedings of the IEEE International Conference on. Neural Networks*, pp. 1942–1948, (1995).

[7] Dorigo, M., Maniezzo, V., and Colorni, A. The ant system: optimization by a colony of cooperating agents. *IEEE Transactions in System, Man and Cybernatics*, B26(1), pp. 29–41, (1996).

[8] Kirkpatrick, S., Gelatt, C., and Vecchi, M. Optimization by simulated annealing. *Science*, 220, pp. 671–680, (1983).

[9] Geem, Z. W., Kim, J. H., and Loganathan, G. V. A new heuristic optimization algorithm: harmony search. *Simulation*, 76(2), pp. 60–68, (2001).

[10] Kaveh, A., and Talatahari, S. A novel heuristic optimization method: charged system search. *Acta Mechanica*, 213, pp. 267–286, (2010a).

[11] Yang, X.S., and Deb, S. Engineering optimisation by cuckoo search, *International Journal of Mathematical Modelling and Numerical Optimization*, 1, pp. 330–43, (2010).

[12] Kaveh, A., and Khayatazad, M. A new meta-heuristic method: ray optimization *Computers and Structures*, 112-113, pp. 283–294, (2012).

[13] Mirjalili, S. The Ant Lion Optimizer, *Advances in Engineering Software*, 83, pp. 80-98, (2015).

[14] Chen, W. N., Zhang, J., Lin, Y., Chen, N., Zhan, Z. H., Chang, H., Li, Y., and Shi, YH. Particle swarm optimization with an aging leader and challengers. *IEEE Transactions on Evolutionary Computing*, 17(2), pp. 241-258, (2013).

[15] Kaveh, A. and Ilchi Ghazaan, M. Hybridized optimization algorithms for design of trusses with multiple natural frequency constraints. *Advances in Engineering Software*, 79, pp. 137-147, (2015).

[16] American Institute of Steel Construction (AISC). *Manual of steel construction–allowable stress design*, 9th Ed. AISC, Chicago, (1989).

[17] American Institute of Steel Construction (AISC). *Manual of steel construction–load and resistance factor design*, 3rd ed., AISC, Chicago, (2001).

[18] Kaveh, A., and Talatahari, S. Optimum design of skeletal structure using imperialist competitive algorithm. *Computers and Structures*, 88, pp. 1220-1229, (2010b).

[19] Dumonteil, P. Simple equations for effective length factors. *Engineering Journal of AISE*, 29(3), pp. 1115, (1992).

[20] Shi, Y., and Eberhart, R. C. A modified particle swarm optimizer. *Proceedings of the IEEE Congress Evolutionary Computing*, pp. 69–73, (1998).

[21] Kaveh, A., and Talatahari, S. Particle swarm optimizer, ant colony strategy and harmony search scheme hybridized for optimization of truss structures. *Computers and Structures*, 87(5–6), pp. 267–283, (2009b).

[22] Kaveh, A., and Talatahari, S. A particle swarm ant colony optimization for truss structures with discrete variables. *Journal of Constructional Steel Research*, 65(8–9), pp. 1558–1568, (2009c).

[23] Kaveh, A., and Talatahari, S. Optimal design of skeletal structures via the charged system search algorithm. *Structural Multidisciplinary Optimization*, 37(6), pp. 893–911, (2010c).

[24] Kaveh, A., Ilchi Ghazaan, M., and Bakhshpoori, T. An improved ray optimization algorithm for design of truss structures. *Periodica Polytechnica,* 57(2), pp. 1-15, (2013).

[25] Hasancebi, O., Çarbas, S., Dog˘an, E., Erdal, F., and Saka, M. P. Performance evaluation of metaheuristic search techniques in the optimum design of real size pin jointed structures. *Computers and Structures*, 87(5–6), pp. 284–302, (2009).

[26] Kaveh, A., and Talatahari, S. A particle swarm ant colony optimization for truss structures with discrete variables. *Journal of Constructional Steel Research*, 65, pp. 1558-1568, (2009a).

[27] Kaveh, A., and Talatahari, S. A discrete Big Bang-Big Crunch algorithm for optimal design of skeletal structures. *Asian Journal of Civil Engineering*, 11(1), pp. 103-122, (2010d).

[28] Degertekin, S. O. Optimum design of steel frames using harmony search algorithm. *Structural Multidisciplinary Optimization*, 36, pp. 393-401, (2008).

[29] Camp, C. V., Bichon, B. J., and Stovall, S. Design of steel frames using ant colony optimization. *Journal of Structural Engineering, ASCE,* pp. 369-379, (2005).

Figure captions

Fig. 1. Schematic of the 120-bar dome shaped truss

Fig. 2. Convergence curves of the 120-bar dome problem

Fig. 3. Schematic of the spatial 582- bar tower

Fig. 4. Stress margins evaluated at the optimum design of the 582-bar tower problem

Fig. 5. Existing displacement in the x-direction for the 582-bar truss

Fig. 6. Existing displacement in the y-direction for the 582-bar truss

Fig. 7. Existing displacement in the z-direction for the 582-bar truss

Fig. 8. Schematic of the 3-bay 15-story frame

Fig. 9. Convergence curves of the 3-bay 15-story frame problem

Fig. 10. Schematic of the 3-bay 24-story frame

Fig. 11. Stress margins evaluated at the optimum design of the 3-bay 24-story frame problem

Fig. 12. Interstory-drift margins evaluated at the optimum design of the 3-bay 24-story frame problem

Table 1. Optimization results obtained for the 120-bar dome problem

Element group	Optimal cross-sectional areas (in^2)				
	Kaveh and Talatahari [18]	Kaveh and Talatahari [23]	Kaveh et al. [24]	Present work	
				ALC-PSO	HALC-PSO
1	3.0275	3.027	3.0252	3.02397	3.02422
2	14.4596	14.606	14.8354	14.72544	14.68930
3	5.2446	5.044	5.1139	5.04683	5.08822
4	3.1413	3.139	3.1305	3.13888	3.13922
5	8.4541	8.543	8.4037	8.53031	8.51643
6	3.3567	3.367	3.3315	3.29159	3.28574
7	2.4947	2.497	2.4968	2.49686	2.49644
Weight (lb)	33,256.2	33,251.9	33,256.48	33,250.18	33,250.01
Average weight (lb)	N/A	N/A	33280.85	33256.02	33256.93
Standard deviation (lb)	N/A	N/A	N/A	5.28	4.16

$1in^2$=$6.4516cm^2$, $1lb$=$4.4482N$

Table 2. Optimization results obtained for the 582-bar tower problem

Element Group	Optimal W-shaped sections			
	Kaveh and Talatahari [26]	Kaveh and Talatahari [27]	Present work	
			ALC-PSO	HALC-PSO
1	W8×24	W8×24	W8×21	W8×21
2	W12×72	W24×68	W14×90	W21×93
3	W8×28	W8×28	W8×24	W8×24
4	W12×58	W18×60	W10×60	W12×58
5	W8×24	W8×24	W8×24	W8×24
6	W8×24	W8×24	W8×21	W8×21
7	W10×49	W21×48	W10×49	W10×45
8	W8×24	W8×24	W8×24	W8×24
9	W8×24	W10×26	W8×21	W8×21
10	W12×40	W14×38	W10×45	W12×50
11	W12×30	W12×30	W8×24	W8×24
12	W12×72	W12×72	W10×68	W21×62
13	W18×76	W21×73	W12×72	W14×74
14	W10×49	W14×53	W12×50	W10×54
15	W14×82	W18×86	W18×76	W18×76
16	W8×31	W8×31	W8×31	W8×31
17	W14×61	W18×60	W14×61	W10×60
18	W8×24	W8×24	W8×24	W8×24
19	W8×21	W16×36	W8×21	W8×21
20	W12×40	W10×39	W12×40	W12×40
21	W8×24	W8×24	W8×24	W8×24
22	W14×22	W8×24	W8×21	W8×21
23	W8×31	W8×31	W8×21	W10×22
24	W8×28	W8×28	W8×24	W8×24
25	W8×21	W8×21	W8×21	W8×21
26	W8×21	W8×24	W8×21	W8×24
27	W8×24	W8×28	W8×24	W6×25
28	W8×28	W14×22	W8×21	W8×21
29	W16×36	W8×24	W8×21	W8×21
30	W8×24	W8×24	W8×24	W8×24
31	W8×21	W14×22	W8×21	W8×21
32	W8×24	W8×24	W8×24	W8×24
Volume (in^3)	1,346,227	1,365,143	1,294,682	1,301,106
Average Volume (in^3)	N/A	N/A	1,304,307	1,312,284
Standard deviation (in^3)	N/A	N/A	4,003	5,895

Table 3. Optimization results obtained for the 3-bay 15-story frame problem

Element Group	Optimal W-shaped sections			
	Kaveh and Talatahari [27]	Kaveh and Talatahari [18]	Present work	
			ALC-PSO	HALC-PSO
1	W24×117	W24×117	W14×99	W14×99
2	W21×132	W21×147	W27×161	W27×161
3	W12×95	W27×84	W27×84	W27×84
4	W18×119	W27×114	W24×104	W24×104
5	W21×93	W14×74	W14×61	W14×61
6	W18×97	W18×86	W30×90	W30×90
7	W18×76	W12×96	W14×48	W18×50
8	W18×65	W24×68	W12×65	W14×61
9	W18×60	W10×39	W8×28	W8×28
10	W10×39	W12×40	W10×39	W10×39
11	W21×48	W21×44	W21×44	W21×44
Weight (lb)	97,689	93,846	87,054	86,916
Average weight (lb)	N/A	N/A	88,114	88,329
Standard deviation (lb)	N/A	N/A	570	904

Table 4. Optimization results obtained for the 3-bay 24-story frame problem

Element Group	Optimal W-shaped sections				
	Camp et al. [29]	Degertekin [28]	Kaveh and Talatahari [18]	Present work	
				ALC-PSO	HALC-PSO
1	W30×90	W30×90	W30×90	W30×90	W30×90
2	W8×18	W10×22	W21×50	W6×15	W6×15
3	W24×55	W18×40	W24×55	W24×55	W24×55
4	W8×21	W12×16	W8×28	W6×8.5	W6×8.5
5	W14×145	W14×176	W14×109	W14×159	W14×159
6	W14×132	W14×176	W14×159	W14×132	W14×132
7	W14×132	W14×132	W14×120	W14×82	W14×109
8	W14×132	W14×109	W14×90	W14×68	W14×74
9	W14×68	W14×82	W14×74	W14×68	W14×61
10	W14×53	W14×74	W14×68	W14×74	W14×74
11	W14×43	W14×34	W14×30	W14×34	W14×30
12	W14×43	W14×22	W14×38	W14×22	W14×22
13	W14×145	W14×145	W14×159	W14×90	W14×90
14	W14×145	W14×132	W14×132	W14×99	W14×99
15	W14×120	W14×109	W14×99	W14×109	W14×90
16	W14×90	W14×82	W14×82	W14×99	W14×90
17	W14×90	W14×61	W14×68	W14×74	W14×74
18	W14×61	W14×48	W14×48	W14×43	W14×38
19	W14×30	W14×30	W14×34	W14×34	W14×38
20	W14×26	W14×22	W14×22	W14×22	W14×22
Weight (lb)	220,465	214,860	212,640	202,410	201,906
Average weight (lb)	229,555	222,620	N/A	208,112	206,463
Standard deviation (lb)	4,561	N/A	N/A	5,075	3,377

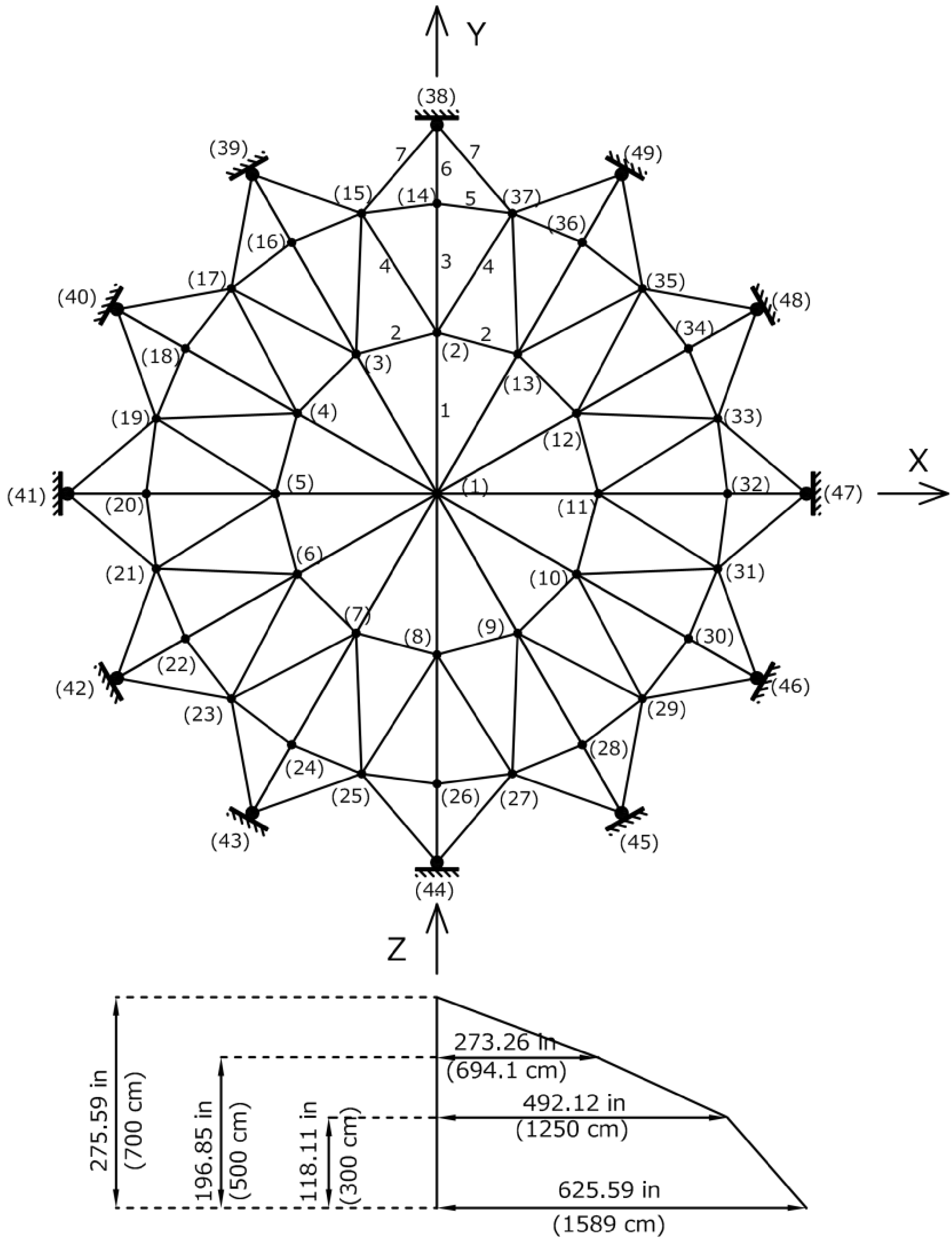

Fig. 1. Schematic of the 120-bar dome shaped truss

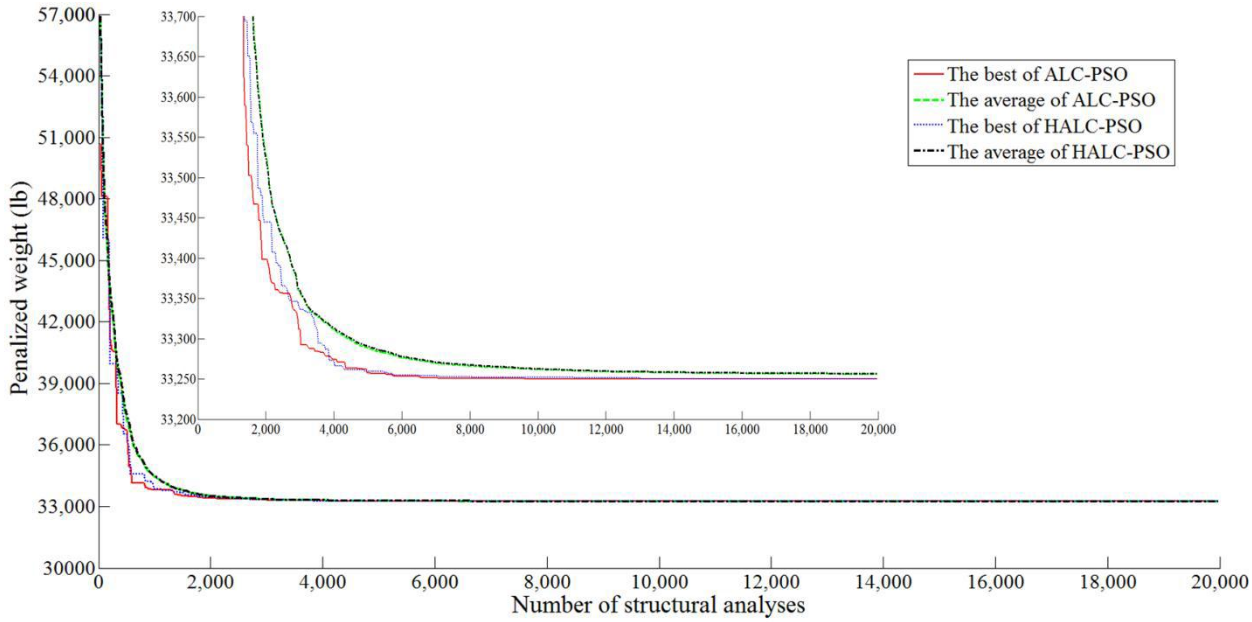

Fig. 2. Convergence curves of the 120-bar dome problem

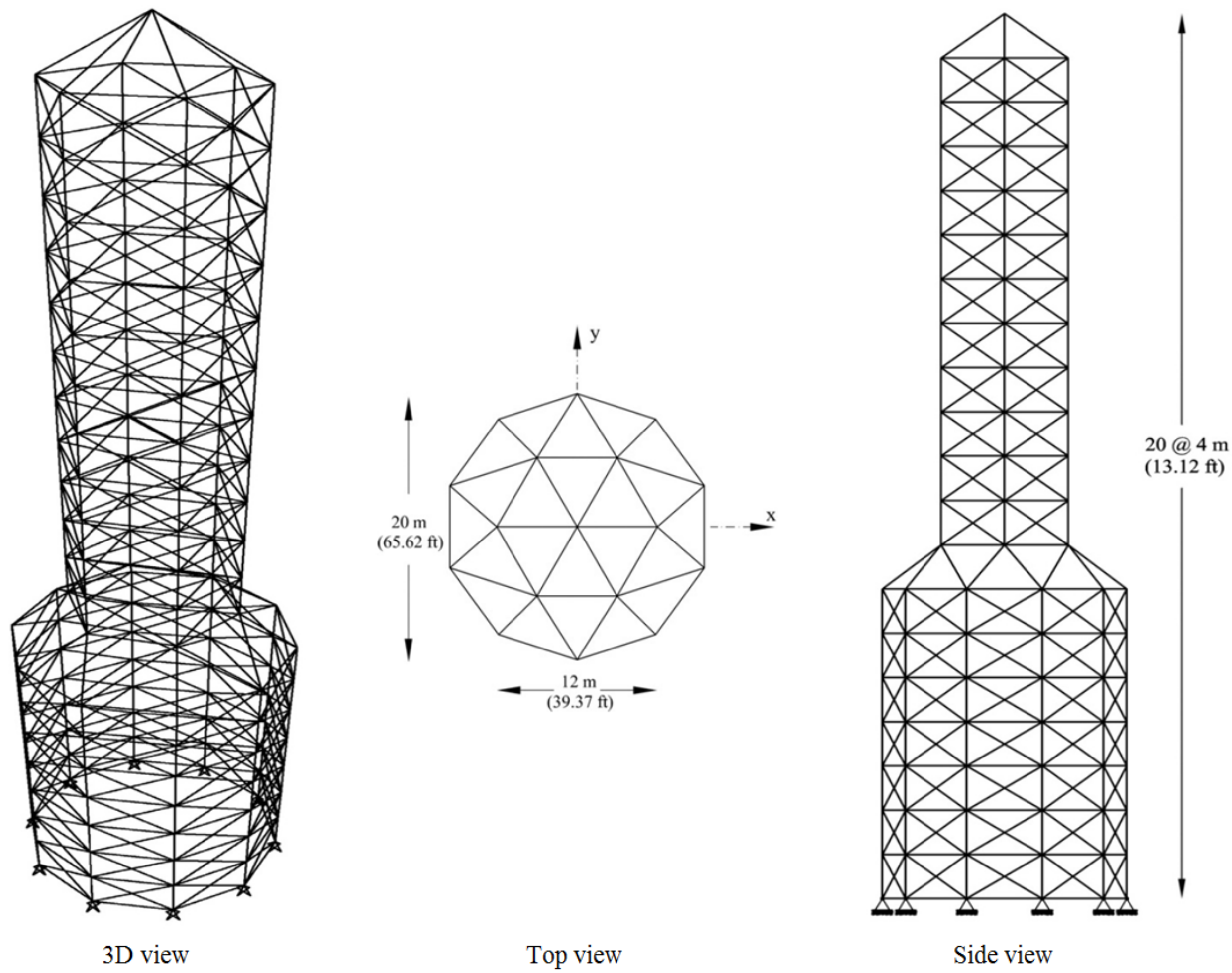

Fig. 3. Schematic of the spatial 582- bar tower

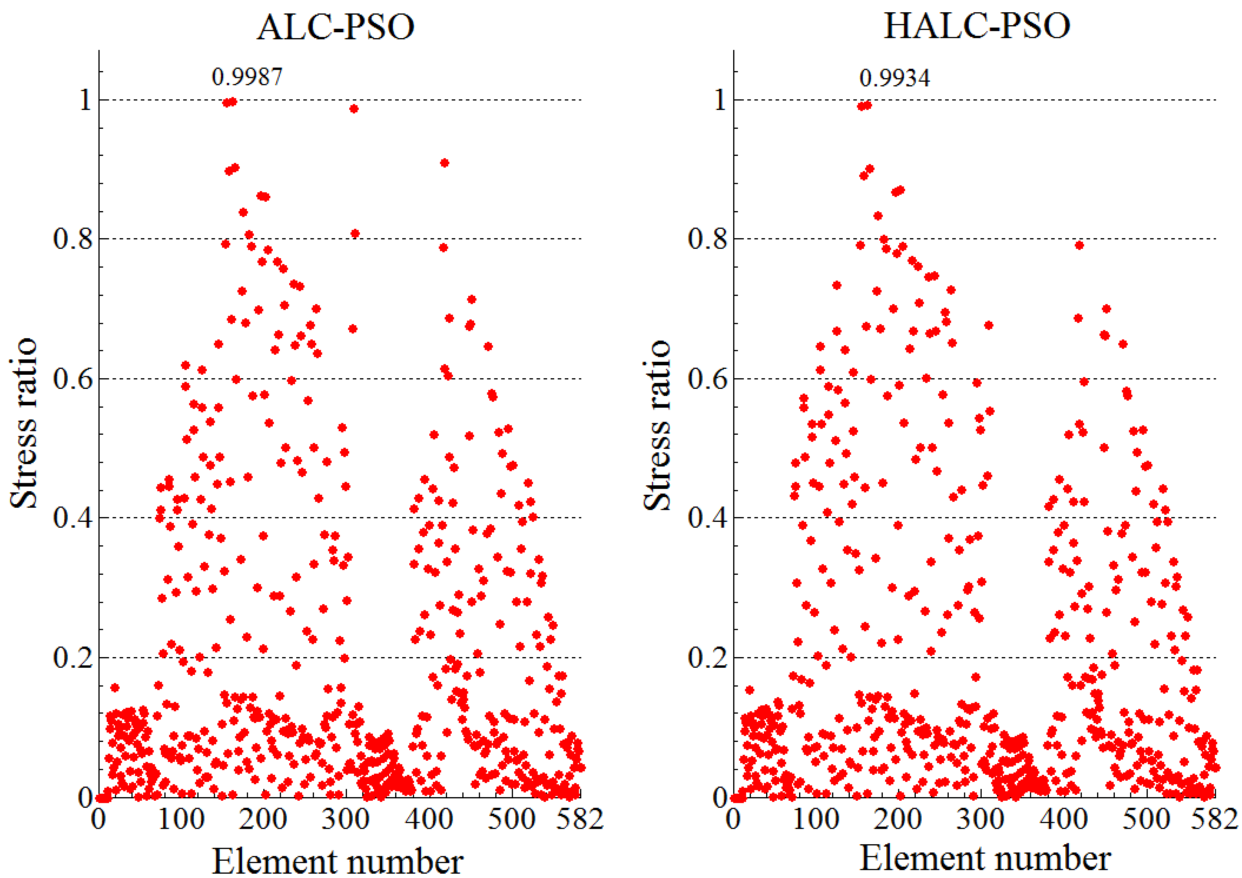

Fig. 4. Stress margins evaluated at the optimum design of the 582-bar tower problem

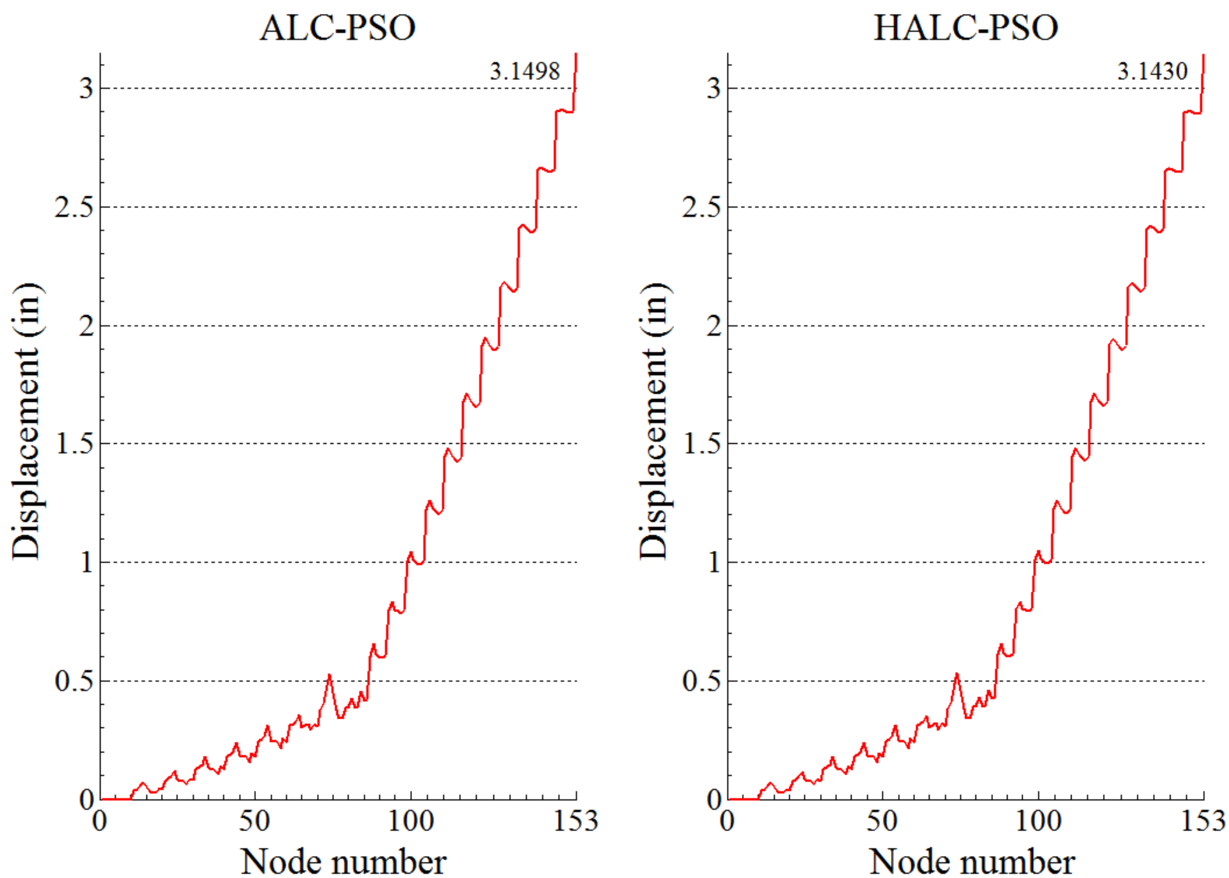

Fig. 5. Existing displacement in the x-direction for the 582-bar truss

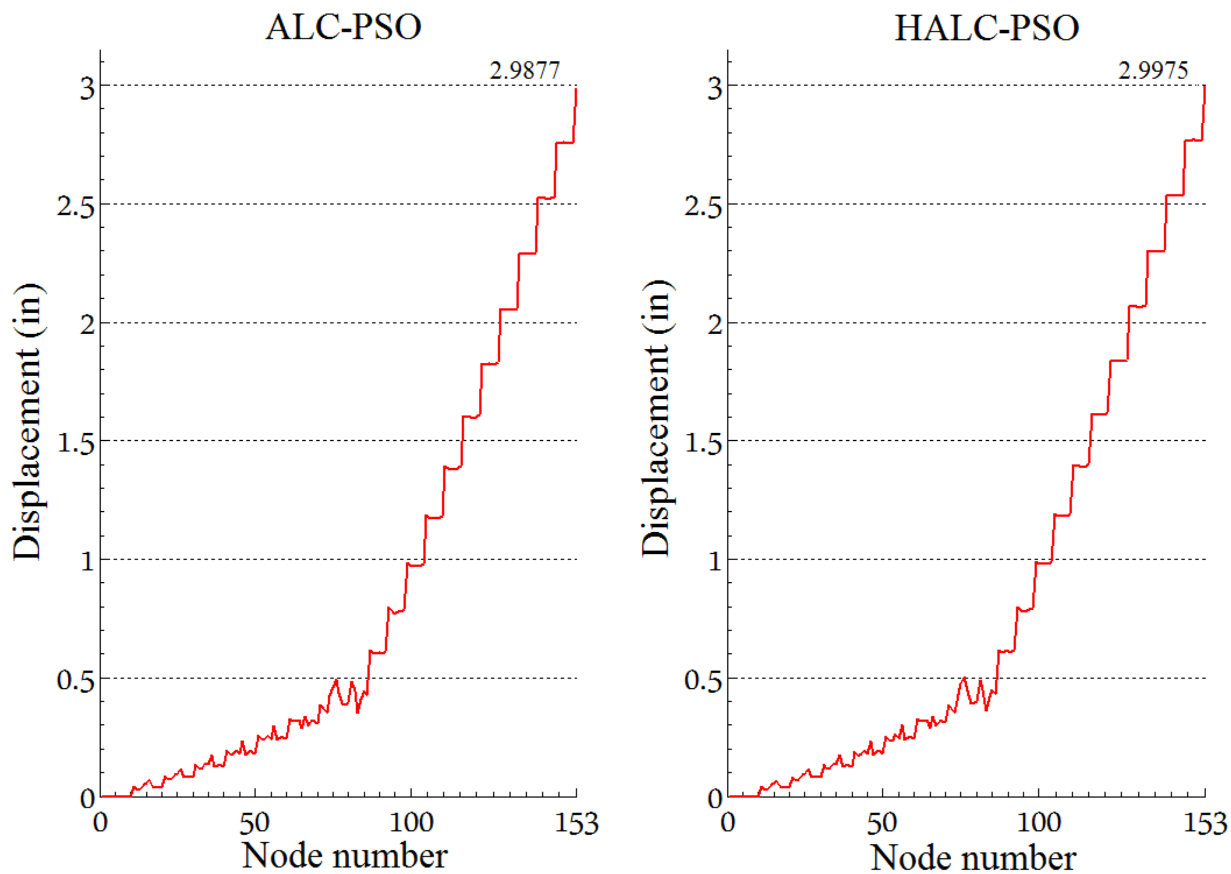

Fig. 6. Existing displacement in the y-direction for the 582-bar truss

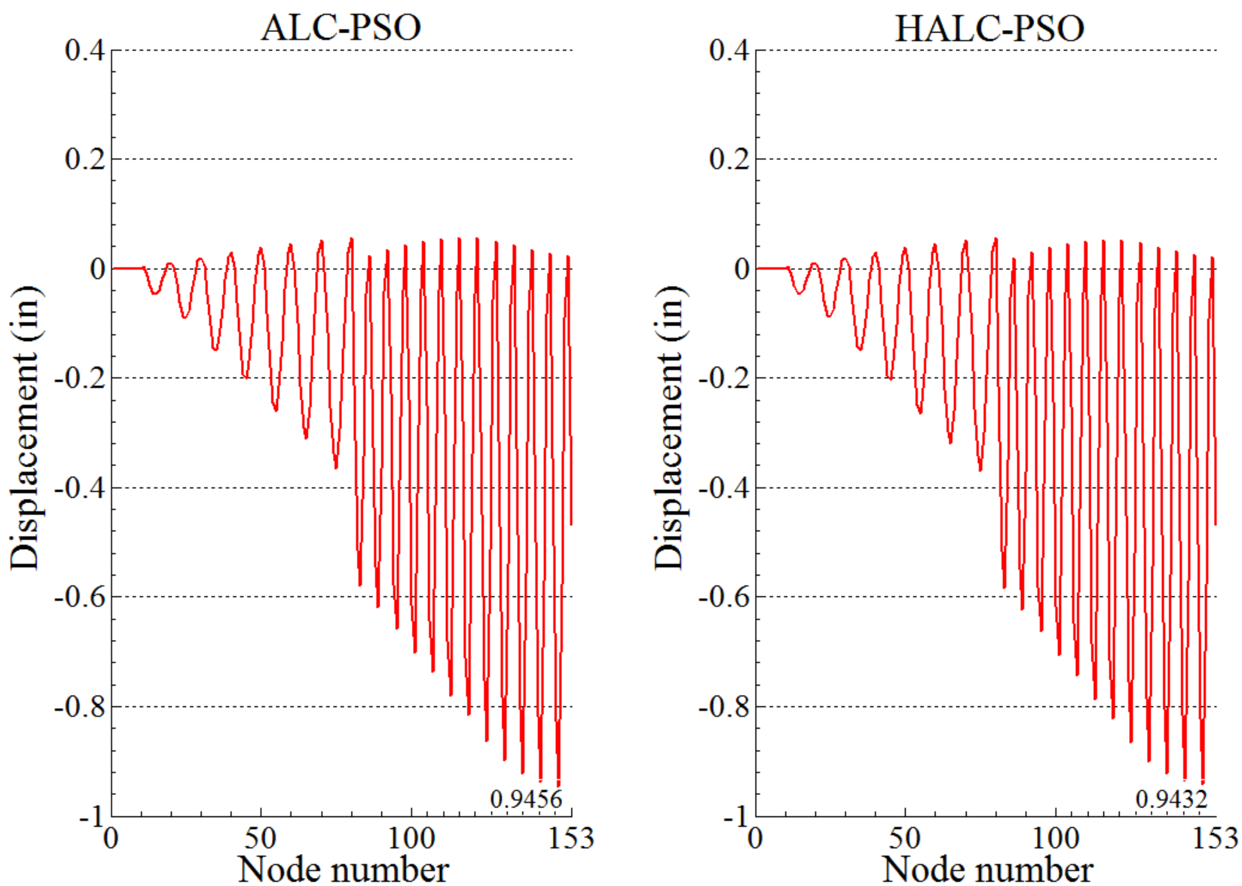

Fig. 7. Existing displacement in the z-direction for the 582-bar truss

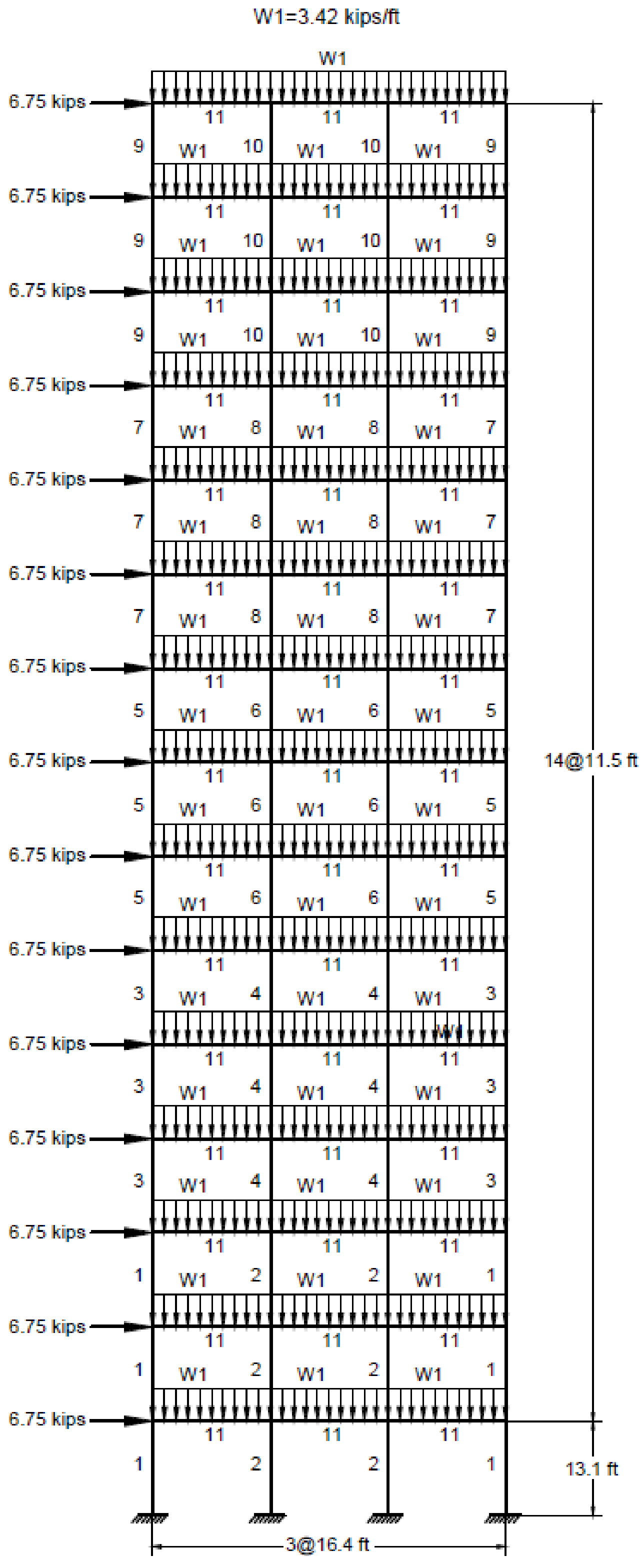

Fig. 8. Schematic of the 3-bay 15-story frame

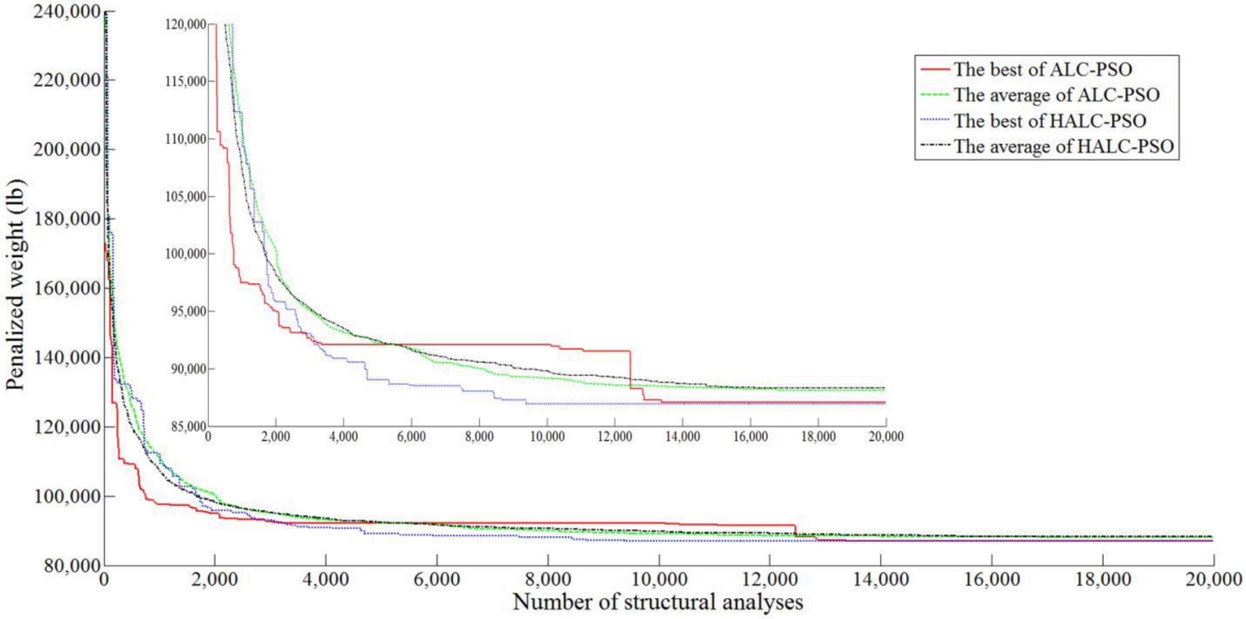

Fig. 9. Convergence curves of the 3-bay 15-story frame problem

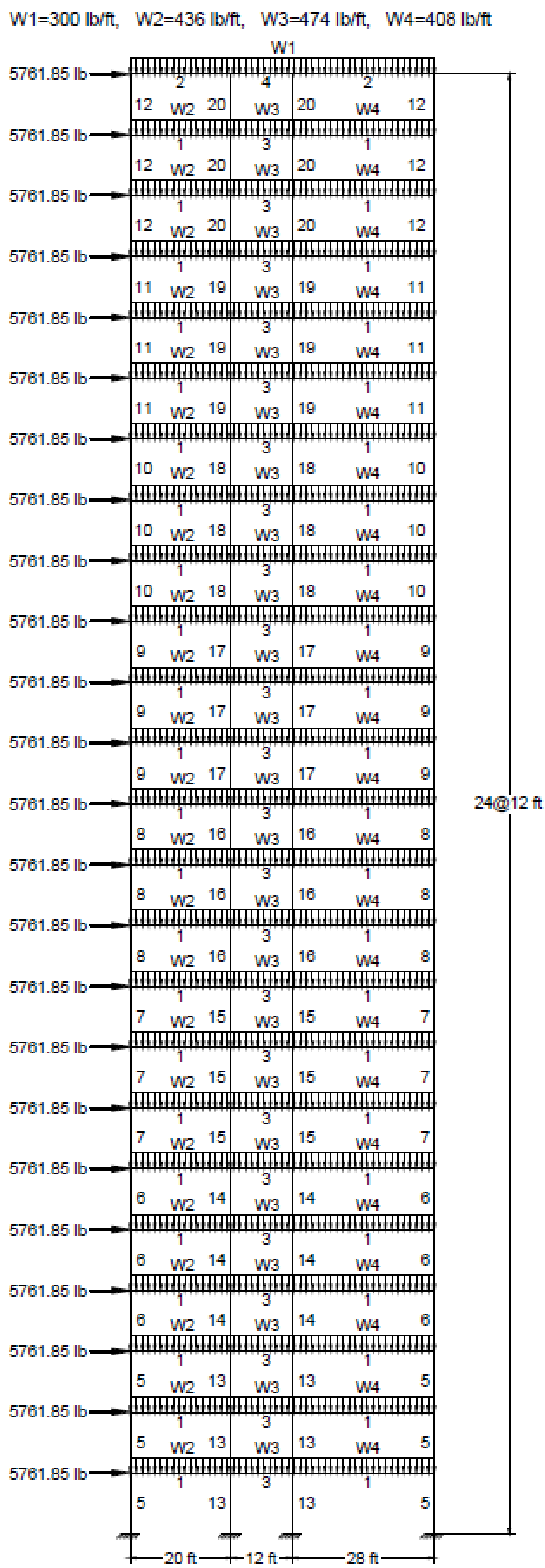

Fig. 10. Schematic of the 3-bay 24-story frame

522

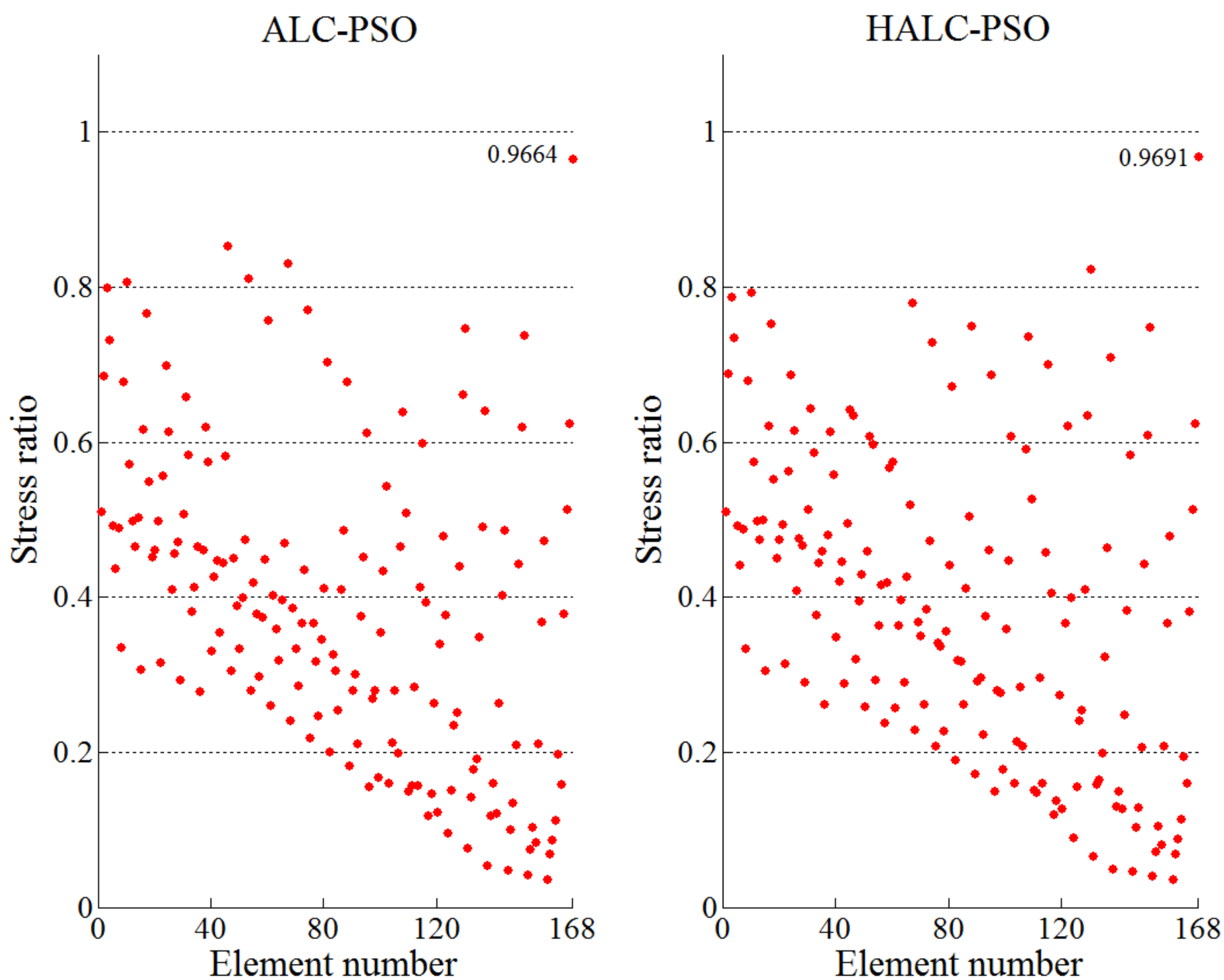

523

524 **Fig. 11.** Stress margins evaluated at the optimum design of the 3-bay 24-story frame problem

525

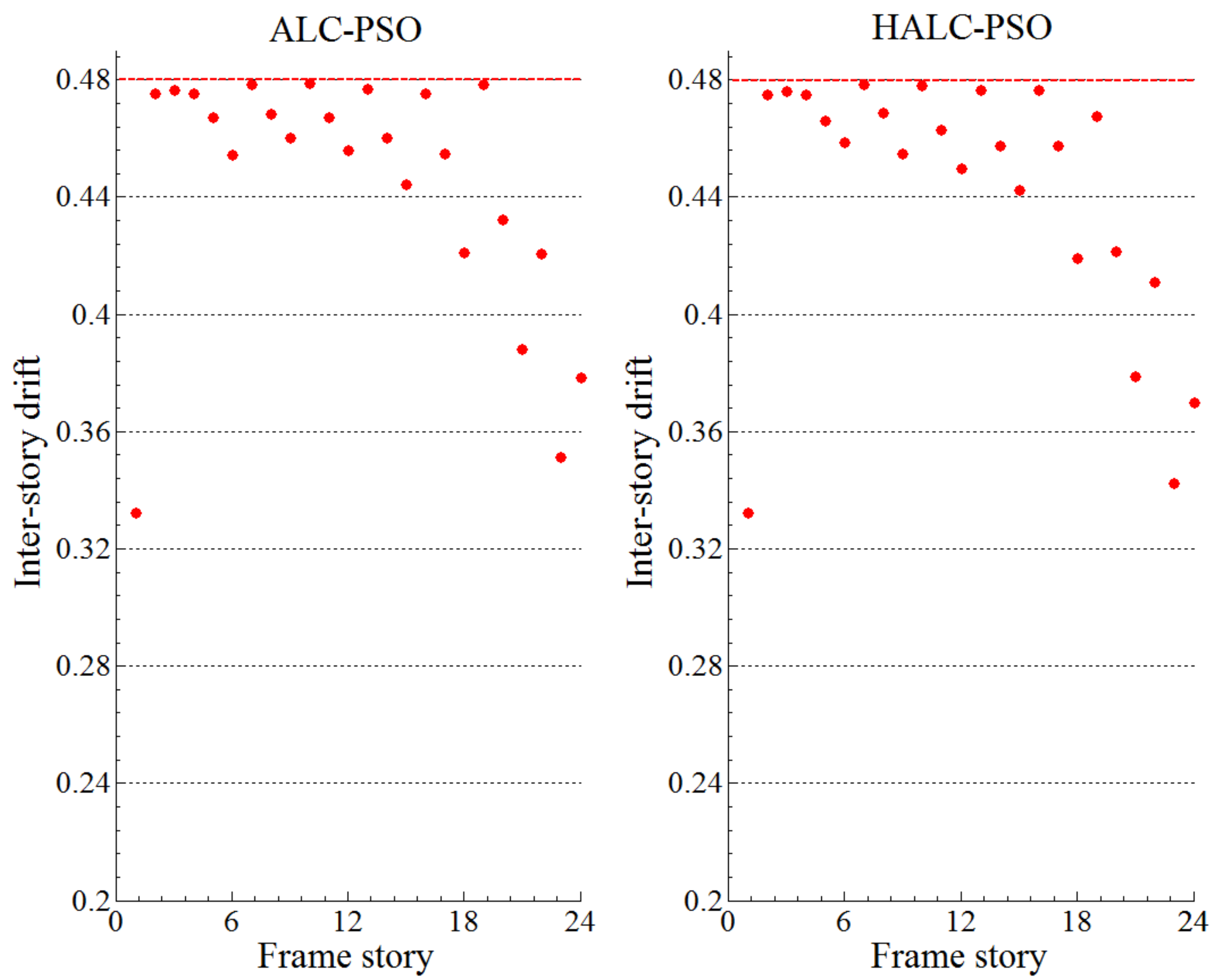

Fig. 12. Interstory-drift margins evaluated at the optimum design of the 3-bay 24-story frame problem